CZ9726896

EQUIVALENT CIRCUIT MODELING OF SPACE CHARGE DOMINATED MAGNETICALLY INSULATED TRANSMISSION LINES

Kazuki HIRAOKA, Mitsuo NAKAJIMA and Kazuhiko HORIOKA
Department of Energy Sciences, Tokyo Institute of Technology
Nagatsuta 4259, Midoriku Yokohama, Japan 226

ABSTRACT

We have developed a new equivalent circuit model for space charge dominated MITLs(Magnetically Insulated Transmission Lines). MITLs under high power operation are dominated with space charge current flowing between anode and cathode. Conventinal equivalent circuit model does not account for space charge effects on power flow. To discuss the power transportation through the high power MITLs, we have modified the model. With this model, we can estimate the effects of space charge current on the power flow efficiency, without using complicated particle code simulations.

1. DEVELOPMENT OF THE MODEL

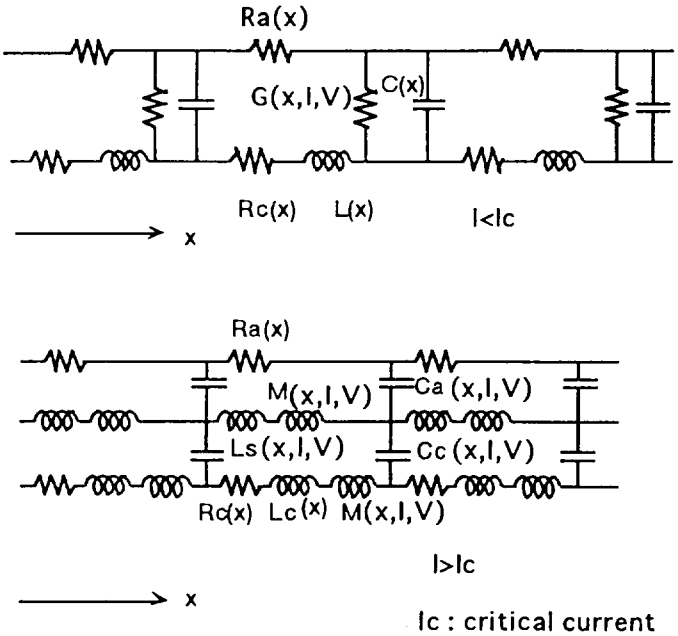

Fig.1 Modified Equivalent Circuit of MITL

In our modeling, as shown schematically in Fig.1, once magnetic insulation is established (I>Ic), the equivalent circuit is replaced by modified circuit that has space charge current path. Here, Ic is the critical current and G is the conductance of space charge limited current flows across the vacuum gap when the insulation is not achieved.

To determine Ic, L, M and C analytically, we use laminer flow theory of space charge flow[1]. It assumes that electrons move in straight trajectories normal to the electric and magnetic field and parallel to the axis. In this theory, solutions for potential, charge desity distribution, and fraction of the current carried by the space charge are obtained self-consistently as follows,

$$I = \frac{I_\alpha}{\ln\left(\frac{r_a}{r_c}\right)} \gamma_m \cdot \left\{ \ln\left(\gamma_m + \sqrt{\gamma_m^2 - 1}\right) + \frac{\gamma_0 - \gamma_m}{\sqrt{\gamma_m^2 - 1}} \right\} \tag{1}$$

$$I_b = \frac{I}{\gamma_m} \tag{2}$$

with

$$\gamma_{0,m} = 1 + \frac{eV_{0,m}}{m_0 c^2} \tag{3}$$

$$I_\alpha = \frac{m_0 c^2}{e}\frac{2\pi}{\mu_0 c} = 8500(A) \tag{4}$$

Here I is the total (anode) current, Vo is the anode potential, Vm is the potential at the edge of the electron sheath, and γ_m is the ratio of total (anode) current I and conduction (boundary) current Ib on the cathode. When the solutions for γ_m of equation (1) are not existing, we regard as the magnetic insulation is not achieved and the minimum value (for V) of right side of equation (1) is chosen for Ic.The distributing profile of space charge flow is assumed as,

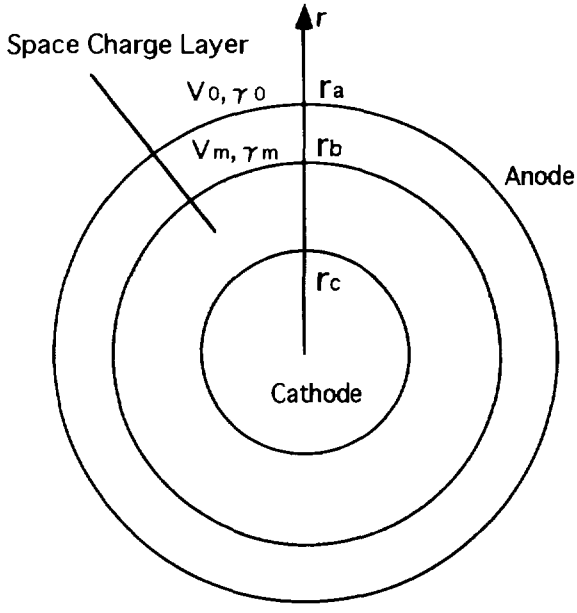

Fig.2 Cross section of cylindrical MITL

$$i(r) = \frac{I}{\gamma_m}\cosh\left(\frac{I}{I_\alpha \gamma_m}\ln\frac{r}{r_c}\right) \tag{5}$$

where r is coodinate of radial direction in the cylindrical MITL, rc and ra is radius of the cathode and anode(Fig.2), i(r) represents the current enclosed with the cylinder of radius r. The outer radius of space charge layer is expressed as

$$r_b = \exp\left(\ln r_a - \frac{\gamma_0 - \gamma_m}{\sqrt{\gamma_m^2 - 1}}\frac{I_\alpha \gamma_m}{I}\right) \tag{6}$$

With these functions, effective inductance Lc, Ls and mutual inductance M can be calculated analytically, as follows,

$$L_c = \frac{\mu_0 l}{2\pi}\ln\frac{r_a}{r_c} \tag{7}$$

$$L_s = \frac{\mu_0 l}{2\pi}\ln\frac{r_a}{r_b} + \frac{1}{I_s}\int_{r_c}^{r_b}\frac{i(r)-I_b}{I_s}\cdot\frac{\mu_0 l}{2\pi r}\cdot\frac{i(r)-I_b}{r}dr \tag{8}$$

$$M = \frac{\mu_0 l}{2\pi}\ln\frac{r_a}{r_b} + \int_{r_c}^{r_b}\frac{i(r)-I_b}{I_s}\cdot\frac{\mu_0 l}{2\pi r}dr \tag{9}$$

where, Is is the space charge current: $I_s = I - I_b = (1-1/\gamma_m)I$, and l is the length of one unit of the equivalent circuit.

The calculation of effective capacitance Ca and Cc depends on some assumptions. At first, we must derive the expression for capasitance dC at radius r and gap distance dr,

$$dC = \frac{2\pi\varepsilon_0 l\, r}{dr} \tag{10}$$

If the currents flowing in the next unit are primed, the current flowing this capasitance is i(r)-i'(r). Using this current and an assumption of the square pulse, the voltage between the edge of electron sheath and the cathode surface is

$$V_m = \int_{r_c}^{r_b} \frac{1}{dC} \int_0^T \left(i(r) - i'(r) \right) dt \tag{11}$$

$$\approx \int_{r_c}^{r_b} \frac{1}{dC} \left(i(r) - i'(r) \right) T \tag{12}$$

$$= \int_{r_c}^{r_b} \frac{1}{2\pi\varepsilon_0 l} \cdot \frac{1}{r} \left(i(r) - i'(r) \right) T\, dr \tag{13}$$

For simplicity, we assume that the ratio i(r) and Ib is nearly equals that of i'(r) and I'b, and Cc is calculated from the next eq.

$$\frac{1}{C_c} = \frac{V_m}{(I_b - I_b')} \approx \int_{r_c}^{r_b} \frac{1}{2\pi\varepsilon_0 l} \cdot \frac{1}{r}\, i(r)\, dr \,/ I_b \tag{14}$$

The capasitance of the vacuum region is obtained by

$$C_a = \frac{2\pi\varepsilon_0 l}{\ln \frac{r_a}{r_b}} \tag{15}$$

The resistance R is electrode resistance when skin depth is about 10^{-5} m .
The conductance G of space charge limited current is usually the product of four functions(16). They are a space-charge-limited Langmuir-Child conductance G_{CL}which depends on voltage and geometry(17), an electric field dependent function f1 accounting for emission turn-on, a smooth function of current f2 which is 1 for zero current and drops to 0 when $I \geq Ic$, and correction function f3 for relativistic effects. Generally to say, the choice of these functions f is arbitrary. In this report, we chose f1, f3 = 1 for simplicity.

$$G = G_{CL} f_1 f_2 f_3 \tag{16}$$

$$G_{CL} = \frac{8\pi\, \varepsilon_0 r_c}{9(r_a - r_c)^2} \sqrt{\frac{2eV}{m}} \tag{17}$$

2. RESULTS

Fig.3(a),(b)are comparisons of simulation results between the equivalent circuit calculation and the PIC simulation and the Flow Impedance model [2]. As shown in Fig.3(a), the effective impedance (V/I) is reduced to about 80% of wave impedance by taking account of space charge current[3] . Because the calculations of PIC and the Flow Impedance model are for positive polarity, they are not strict comparison, but qualitative characteristics are fairly expressed with our model. With some modifications, our model can treat positive polarity.

3. CONCLUDING REMARKS

We have developed a new equivalent circuit model of MITLs which includes space charge effects. Results obtained with this model are compared to those by PIC and Flow Impedane model simulations. The qualitative agreement between the simplified calculation and the results of PIC simulation is fairly good. The CPU time for the calculations is only one minute or so by an average level personal computer (with Power PC603 75MHz unit).

REFERENCES

[1] John M.Creedon, J.Appl.Phys. 46, p.2946 (1975).

[2] C. W. Mendel, Jr. and S. E. Rosenthal , Proc.10th Int.Conf.High Power Particle Beams, p276 (1994)

[3] K.Hiraoka,K.Horioka,M.Nakajima and T.Aoki , NIFS-PROC-24 (1996 now printing)

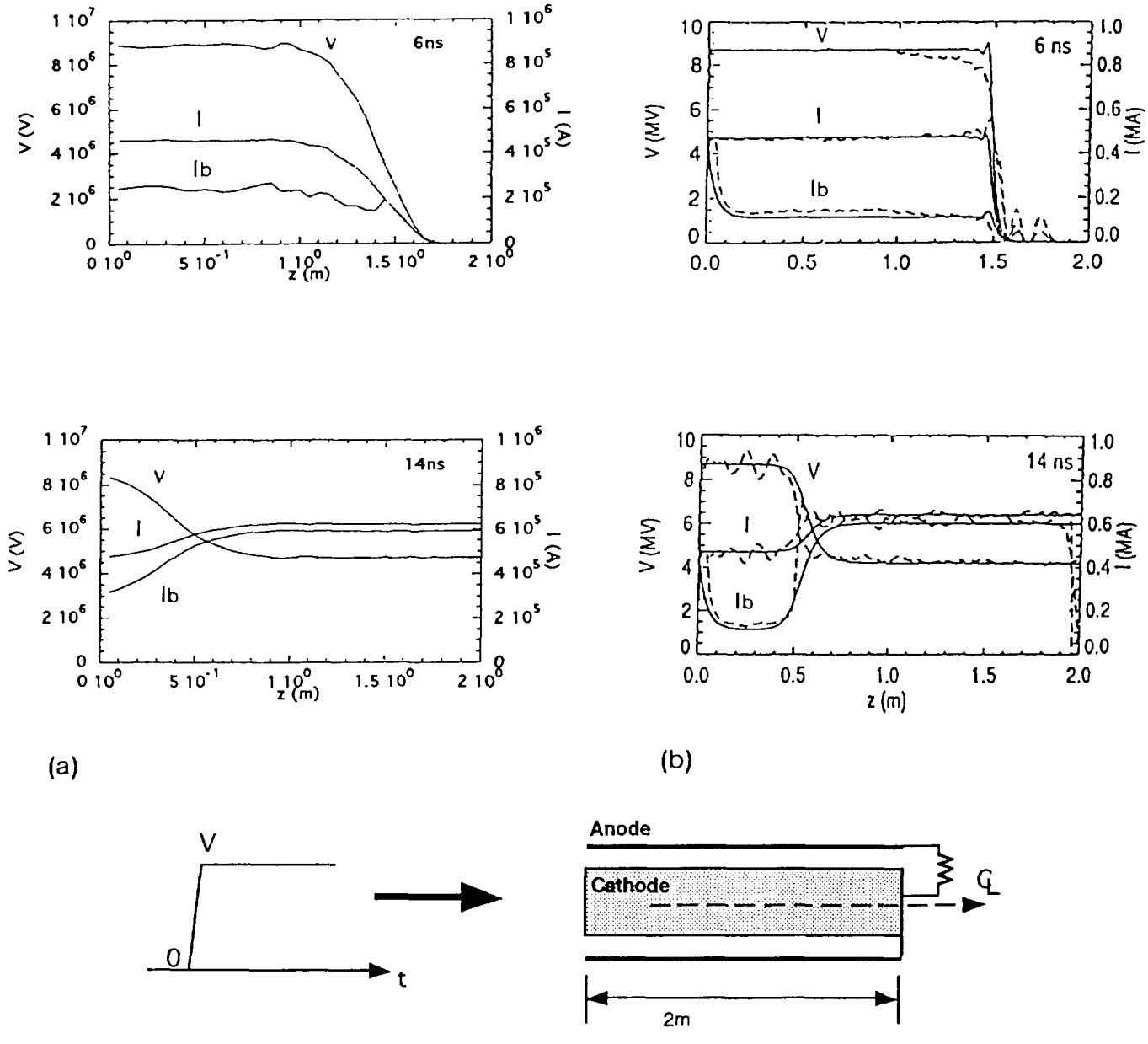

Fig.3 (a)The model and (b) PIC(dashed) and Flow Impedance model(solid) caluculations for a step voltage in a 24.3Ω, 2m long MITL.

CONTRIBUTED PAPERS P-4

Astrophysics

Beam and Plasma Diagnostics

Inertial Confinement Fusion

Ion Beam Physics

Ion Diodes

Ion Rings

Ion Sources

Plasma Opening Switches

Solid State Opening Switches

Targets

HIGH-VOLTAGE SPACE TETHER FOR PARTICLE SCATTERING IN EARTH'S RADIATION BELTS

V. V. Danilov
Krasnoyarsk State University, 660041 Krasnoyarsk, Russia
V. V. Mirnov[1], *D. Üçer*
Middle East Technical University, 06531, Ankara, Turkey

1 Introduction

New applications of space tethers are discussed in relation with the idea [1] of an active experiment, in the Earth's radiation belts. Two long (about 10 km long each) strings of radius $r_p \sim 1mm$ made from cevlar and coated with a highly conducting material are supposed to be tethered in opposite directions between the main satellite and two small subsatellites, flying through the ERB in equatorial plane. High potential difference $\phi_p \sim 1\ MV$ is applied between the tethers, by means of a compact high voltage generator carried by the main satellite. The tethers can effectively scatter the high energy particles into loss cone, providing a control of particle life time in ERB. This high-voltage satellite system can be used for precipitation of charge particles from man-made radiation belts, affecting the ozone layer depletion and other active experiments in space such as ARAKS, CRRES, *etc.*. Electrodynamic aspects of the tethers and technical requirements for the generator are the subject of the consideration below.

2 Structure of the sheath layer

The high energy particles are scattered due to the sheath layer formed around the tethers by relatively cold plasma ($n = 10^2\ cm^{-3}$, $T = 100\ eV$) existing in ERB. The problem of evaluation of the potential profile is quite similar to that studied in the standard double Langmuir probe theory [2]. Specific feature of our case is extremely high potential of the probe $p = e\phi_p/kT \sim 10^4$ and high aspect ratio $R = r_s/r_p \sim 10^8$, that strongly effects on the value of sheath radius r_s ($r_s \sim 0.5\ km$) and current collected by the tethers. Since this range of parameters is not widely discussed in publications, potential and current calculations are reproduced below by making use of some rough iteration technics.

With high voltage applied between the tethers two oppositely charged sheaths are formed around the strings. Positively charged string attracts the electrons and, correspondingly, the area around it is negatively charged, while the ions are attracted by another string, which is surrounded by positively charged layer. In stationary state electron and ion currents has to be equal to each other. Since the calculations related to ion and electron sheaths are quite similar, we will focus attention on the ion case only.

The typical ion velocity in the sheath area is $v_s = \sqrt{2e\phi_p/m_i} \sim 1.4\ 10^7\ m/sec$, transit (bounce) time $t_s = 2r_s/v_s \sim 10^{-4}\ sec$, Larmor radius is large enough, $r_{Li} \sim 100\ km$, that allows to neglect effect of magnetic field on particle motion. Electrostatic potential is, therefore, axisymmetric with respect to the tethers and with the assumption of an infinitely long string it varies along r only, where z axis of the cylindrical reference frame (r, α, z) is chosen to be along the strings. The particle dynamics is governed by the integrals of energy

[1] on leave from Budker Institute of Nuclear Physics, Novosibirsk, 630090, Russia

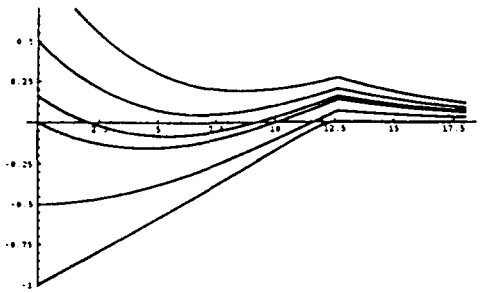

Figure 1: The graphs of $U_{eff}(M,r)$ (normalized to $e\phi_p$) versus $\ln r/r_p$ for a few values of M. The lower curve ($M = 0$) illustrates a typical behavior of electrostatic potential in sheath area

$E = m_i v^2/2 + e\phi(r)$ and angular momentum $M = mvr\sin\alpha$. With the help of conservation laws 3D problem of particle motion is reduced to 1D problem, which corresponds to the radial motion with effective potential energy $U_{eff}(M,r) = M^2/2mr^2 + e\phi(r)$. Analyzing graphs of U_{eff} illustrated in Fig.1, one can classify particles in accordance with their integral of motion into three main groups - locally trapped, absorbed and transit ions.

Ion distribution function is described by Vlasov-Maxwell equation with boundary condition at $r \to \infty$, implying that particles flying toward the string ($v_r < 0$) have a Maxwell distribution function: $f = f_m = n_\infty(m/2\pi kT)^{3/2}\exp(-mv^2/2kT)$, and boundary condition on the string surface ($r = r_p$) assuming that all particles reaching this surface become absorbed without any emission. Then, ion current density and ion density can be evaluated by integration of distribution function over the relevant region in velocity space.

The critical issue of ion density calculation is the distribution function of the locally trapped particles. If significant amount of these particles is accumulated and trapped in the sheath area, then electrostatic potential turns out to be shielded in the narrow vicinity of the string that strongly decreases scattering efficiency. Because of this reason some mechanism (AC current or other one) for removing and pumping of trapped particles has to be provided. In our further consideration we will analyze the most favorable case assuming that trapped particle distribution function equals to zero.

With the help of some simplifications based on the fact that the maximum of U_{eff} is well localized near the sheath boundary, $r_{max} \simeq r_s$ (see Fig.1), expression for ion density inside the sheath area can be written as follows:

$$n_i(r) = \frac{n_\infty}{\pi}\left[\int_{\alpha_1}^{\alpha_2} d\alpha \exp\left(-\frac{p\phi(r)\sin^2\alpha}{1-(r^2/r_s^2)\sin^2\alpha}\right) + \int_{\alpha_2}^{\pi} d\alpha \exp\left(\frac{p+p\phi(r)(r^2/r_p^2)\sin^2\alpha}{1-(r^2/r_p^2)\sin^2\alpha}\right)\right] \tag{1}$$

where $\alpha_1 = \arcsin[r_p/r]$, $\alpha_2 = arcsin[(r_s/r)\sqrt{1-\phi(r)(R^2-1)}\,]$, $\phi(r)$ is a potential, normalized to ϕ_p. Since electrons are strongly repulsed by the negatively charged tether, their density is described by Boltzman distribution: $n_e(r) = n_\infty\exp[-p\phi(r)]$. Then, Poisson's equation has been treated numerically yielding potential profile. First approximation for $\phi(r)$ was found due to simplification that ion density is a *const*, $n_i(r) = n_\infty$. Making use of initial condition on the string surface, $\phi(r_p) = 1$, and varying initial slope at this point, the sheath radius r_s has been evaluated in the way allowing to satisfy with two other conditions, $\phi(r_s) = d\phi(r_s)/dr = 0$.

The profile obtained is then substituted into (1) to calculate corrected dependence $n_i(r)$. Corrected function turns out to be *const* ($n_i = n_\infty$) everywhere, except narrow vicinity of the string ($0 \le \ln(r/r_p) \le 5$), where ion density gradually decreases reaching value $n(r_p) = n_\infty/2$ on string surface. Since this area makes small contribution in r.h.s. of Poisson's equation, second iteration for $\phi(r)$ proved to be close to the first one, shown in Fig.1. With the accuracy needed for the treatment of the scattering problem this function

ϕ_p, MV	0.1	0.5	1.0	1.5	2.0	2.5	3.0
r_s, km	0.10	0.24	0.31	0.38	0,46	0.50	0.54
$J, 10^{-3}A$	1.4	3.2	4.5	5.5	6.4	7.2	7.8
P, kW	0.14	1.60	4.50	8.25	12.8	18.0	23.4

Table 1: The dependences of sheath radius r_s, collected current ($L = 10\ km$), and electrical power on applied potential difference ϕ_p

can be approximated as follows:

$$\phi(r) = \begin{cases} \phi_p\,[(\ln(r/r_p)/\ln R) - 1] & r \le r_s \\ 0 & r \ge r_s \end{cases} \tag{2}$$

Calculations of ion current density are not sensitive to the locally trapped particles. Evaluating corresponding integrals, one obtains:

$$j_r = n_\infty \left(\frac{2kT}{\pi m_i}\right)^{1/2} \frac{r_p}{r} \left(\exp p \int_{\sqrt{p}}^{\infty} x^2 \exp(-x^2)dx + R\int_0^{p/R} x^2 \exp(-x^2)dx\right) \tag{3}$$

In the case of practical interest, $p \gg 1, R \gg 1$, expression (3) can be simplified yielding total current collected by the negative tether: $J_i = 2en_\infty r_p L(2e\phi_p/m_i)^{1/2}$. Similar expression for electron current is inversely proportional to $m_e^{1/2}$. Equating electron and ion currents yields potential of the strings with respect to infinity: $\phi_+ = \phi_p/(1 + m_i/m_e) \sim 500\ V, \phi_- = \phi_p/(1 + m_e/m_i) \sim \phi_p$, showing that only negative string can effectively scatter high energy component. The summary of the results related to electrical characteristics of the tethers is given in Table 1.

3 The scattering of high energy particles

Because the scattering angle of high energy particles caused by their collisions with the sheath layer is small, Fokker-Planck equation can be used for the treatment of particle losses from ERB. In the reference frame (x, y, z), z axis is supposed to be along magnetic field while the string is oriented along y axis. During a process of scattering the absolute value of perpendicular velocity, $\vec{v}_\perp = v_x\vec{e}_x + v_z\vec{e}_z$, and the value of v_y are conserved. Then, the increment of $\vec{v}_\perp$ is: $|\Delta\vec{v}_\perp| = 2v_\perp \sin(\alpha/2)$, where α is the scattering angle in xz plane. With the help of (2) α is found to be the following function of impact parameter ρ:

$$\alpha = \frac{2e|\phi_p|}{mv_\perp^2}\frac{1}{\ln R}\arctan\sqrt{r_s^2/\rho^2 - 1} \tag{4}$$

In order to find the rate of diffusion into the loss cone, θ component of velocity increment $\Delta v_\theta = 2\sin\frac{\alpha}{2}\cos\varphi$ is analyzed, where θ is a pitch angle, φ is azimuthal angle in a spherical reference frame. To evaluate average moment $< \Delta\theta^2 >=< \Delta v_\theta{}^2 > /v^2$, which defines the rate of losses, we take into account many microcollisions of test particle with the string, resulting from it's bounce motion along field lines and slow revolution of satellite in equatorial plane. Then, averaging can be done by means of integration over ρ ($-r_s \le \rho \le r_s$), while v, θ and $\sin\varphi = x/r_L$ are fixed, where x is a coordinate of guiding center, $r_L = mv\sin\theta/eB$ is

H, km	protons $A_{loss}(sec^{-1})$	protons E_0, MeV	protons $q_{total}(sec^{-1})$	electrons A_{loss} (sec^{-1})	electrons E_0, MeV	electrons $q_{total}(sec^{-1})$
2000	4.3×10^9	64.2	1.8×10^{15}	2.5×10^{17}	0.28	1.4×10^{18}
6000	9.9×10^{11}	17.7	3.1×10^{16}	1.2×10^{17}	0.22	3.7×10^{17}
10000	7.8×10^{15}	1.0	2.5×10^{21}	2.3×10^{16}	0.3	1.5×10^{17}
20000	1.9×10^{17}	0.25	8.0×10^{17}	9.1×10^{15}	0.57	2.5×10^{17}

Table 2: The characteristics of the distribution functions of loss-fluxes for the different radiation belts ($\phi_p = 1\ MV, L = 10\ km, r_s = 0.32\ km$)

a Larmor radius.

$$< \Delta\theta^2 >= 4(\pi - 2)\frac{Lr_s v}{2\pi r_L l\ (2\pi R_s)} \left(\frac{2e\phi_p}{mv^2 \ln R}\right)^2 \frac{1 - (x^2/r_L^2)}{\left(1 - (x^2/r_L^2)\sin^2\theta\right)^{3/2}} \tag{5}$$

Here l is a length of magnetic field line, R_s is a radius of satellite orbit.

Making use of Fokker-Planck equation the rate of particle losses from ERB has been evaluated. It results in the energy distributions of loss-fluxes, which represent the number of particles escaping from ERB per unit time and having energies greater than E. The fluxes are averaged over the time interval which is much longer then the period of satellite revolution over the Earth. They are also integrated over the area, thus, giving the rate of total amount of particles falling down to the Earth's surface. Using the experimental date obtained through the measurements of the fluxes of trapped particles in radiation belts, yields the tail of distribution function of escaping particles:

$$\frac{dN}{dt}(> E) = A_{loss}(E_0/E)^2 \exp(-E/E_0) \tag{6}$$

where factors E_0 and A_{loss} are given in Table.2. Note that in the case of proton belt localized at the altitude $H = 10000\ km$ the distribution function (6) turns out to be: $A_{loss}(E_0/E)^{5.5}$.

4 Conclusion

The above calculations show that the loss rate $dN(E)/dt$ depends on the distribution function of the trapped particles and applied potential difference. This allows to use the scattering center for the measurements of high energy particle distribution function. If potential difference can be varied in a wide range, both cold plasma and high energy particles' parameters can be measured with the same space tethers used as a diagnostic probe. For this purpose tunable high-voltage $0.1\ MV \leq \phi_p \leq 2\ MV$, low power $0.1\ KW \leq P \leq 10\ KW$, compact (weight $\leq 1\ T$) DC generator is needed. Some other opportunities appear in AC case.

References

[1] Vasilyev Yu. V., V. V. Danilov,*"Active experiment in space: man-made control of particle precipitation from the Earth's radiation belts using high-voltage string system"*, Dokl. RAN, (1995) **342**

[2] Swift J. D., M. J.Schwar, *Electrical Probes for Plasma Diagnostics*, New York: American Company, 1968.

ELECTRON BEAMS IN LARGE CORONAL LOOPS

M. Karlický[1], H. Aurass [2], G. Mann [2]

1 Astronomical Institute of the Academy of Sciences of the Czech Republic, 251 65 Ondřejov, Czech Republic

2 Astrophysikalisches Institut Potsdam, Observatorium für solare Radioastronomie, Telegrafenberg A31, 14473 Potsdam, Germany

Abstract

The type U(N) radio burst observed at February 23, 1993 is presented. Using a 1-D test particle model, this radio burst is modeled as an electron beam propagating in a large coronal loop. For modeling of transport processes Coulomb collisions, mirroring of electrons in the loop magnetic field, and scattering in zones of enhanced whistler wave turbulence are taken into account. In the model electrons are injected upwards along the loop axis in one leg. In the zone of whistler turbulence near the loop top the original beam is splitted up into two beams propagating from the top back and forward into both loop legs. It explains two widely separated radio sources observed during the descending branch of U burst spectra.

Introduction

During the flare process electron beams travel along open as well as along closed magnetic field lines and they generate type III or type U bursts in the radio spectra [1]. Type U bursts consist of a type III like rising branch that turns over into a descending (reverse drift) branch. Occasionally a type U burst is followed by a new rising branch, forming a burst spectrum reminding the letter "N". Such bursts are called type U(N) bursts [2]. All these radio bursts provide a diagnostic tool for studying particle acceleration, injection and propagation in the solar corona.

Observations of the February 23, 1993 U(N) type radio burst

Figure 1A shows the type U(N) burst spectrum (spectrometer of the Observatory of Solar Radioastronomy of the Astrophysikalisches Institut Potsdam in Tremsdorf) starting 18 min after a subflare in NOAA AR 7433 (N12 E40, Solar Geophysical Data). The main features of the radio source configuration are shown in the one-dimensional scans and the flux curves of the different subsources given in Figure 1B (Nançay multifrequency radio heliograph of the Paris-Meudon Observatory, NRH). The gross source site pattern confirms the model of an electron beam propagating in a closed coronal loop: a brightening at a given site (the leg into which the beam is injected) during the rising branch in the spectrum (U_{up} in Figure 1B) followed by a remote brightening during the descending branch in the spectrum (U_{down} in Figure 1B). The time difference between ascending and descending branches of the U burst at 236.6 MHz is 2.7 s. The N branch of the spectrum (N in Figure 1) occurs nearly at the site of the descending U branch source with 4.2 s time delay. Note that the N branch signature is more diffuse in comparison with the ascending

U branch. The burst sources are located near a large coronal soft X-ray loop rooted in NOAA AR 7433. For details and further examples see [7].

Looking more carefully to the details of Figure 1B some additional weak sources become visible just in the beginning of the brightening of the main U descending and N branch sources. These faint brightenings are situated definitely at the source site of the rising U burst branch, this means near the beam injection site.

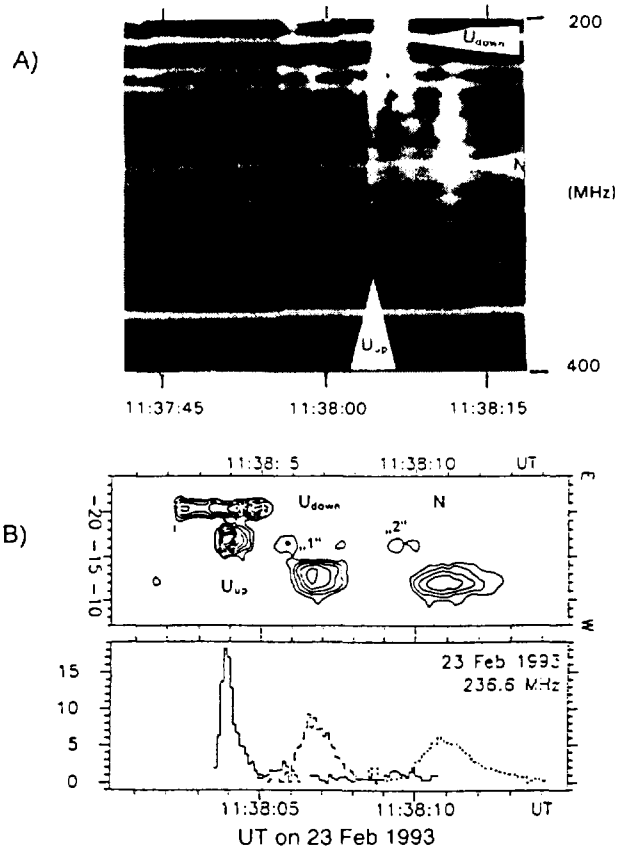

Figure 1. The type U(N) solar radio burst on February 23, 1993 as observed by the Tremsdorf spectrometer (Figure A) and by the Nançay multifrequency radio heliograph (Figure B, top one-dimensional scan at 236.6 MHz; bottom the flux of the subsources in arbitrary units (according to [7]). Continous line - ascending U burst branch; dashed line - descending U burst branch; dotted line - N burst branch).

Model

For modeling of this observations we use a 1-D test particle model [3], in which the trajectories of numerical electrons are computed in a large coronal loop. As concerns the energy losses and the pitch angle changes of individual electrons three effects are taken into consideration:

1. The energy losses and pitch angle scattering of electrons due to Coulomb collisions with the surrounding plasma are calculated by a Monte Carlo method as in [4].
2. Magnetic mirroring effects are included similarly as in [5] considering the conservation

of the electron magnetic moment.

3. Scattering at a zone of enhanced whistler turbulence was computed by Monte Carlo method as suggested in [6]. We compute the coefficients of Fokker-Plank equation in the following form:

$$D^w_{\mu\mu} = \left(\frac{\pi^2 e}{m_e c}\left(\frac{2n}{n+1}\right)\frac{W^{tot}_w}{B}\frac{1}{\gamma}\left(\frac{\beta\gamma}{1836\beta_a}\right)^{n-1}\right) \mid \mu \mid^{n-1} (1-\mu^2), \tag{1}$$

$$D^w_{\mu} = \left(\frac{\pi^2 e}{m_e c}\left(\frac{2n}{n+1}\right)\frac{W^{tot}_w}{B}\frac{1}{\gamma}\left(\frac{\beta\gamma}{1836\beta_a}\right)^{n-1}\right) sign(\mu)((n-1)(1-\mu^2) \mid \mu \mid^{n-2} - 2 \mid \mu \mid^{n}). \tag{2}$$

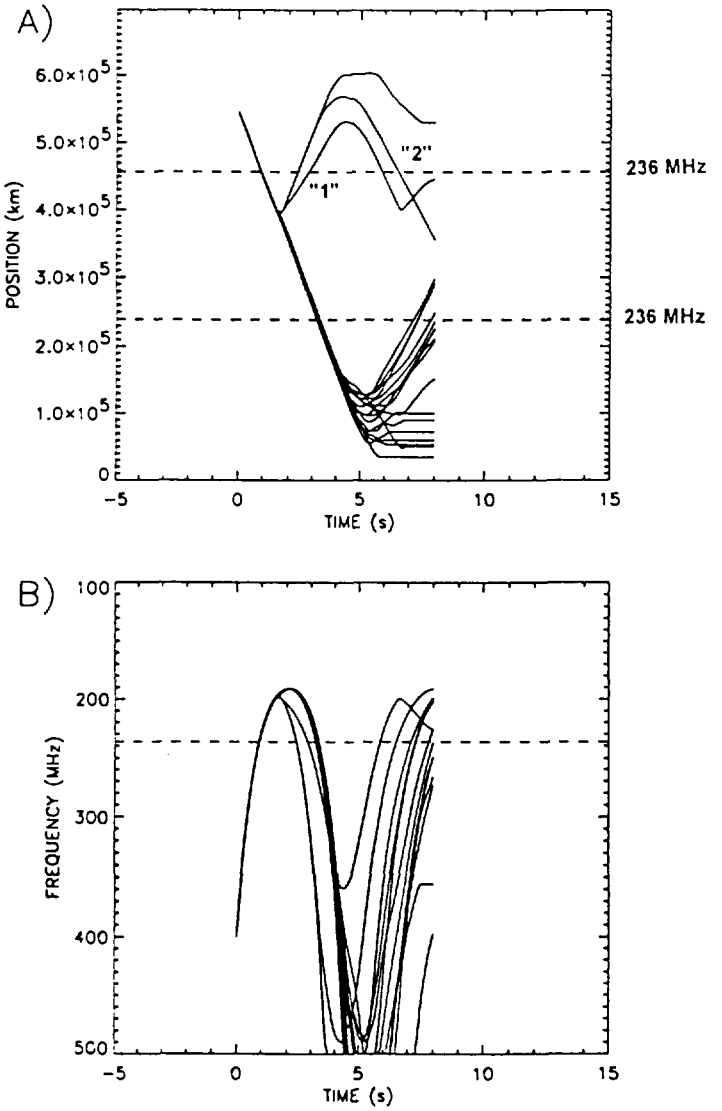

Figure 2. The numerical simulation of the February 23, 1993 U(N) burst. The trajectories of 20 numerical electrons in the distance vs time (A) and the frequency vs time (B) plots for the case when Coulomb collisions, mirroring and scattering of electrons at whistler turbulence zone near the loop top are considered.

Now, let us model the presented observation. The length of the semi-circular loop is estimated to about 1 solar radius from radio heliographic and YOHKOH observations. Assuming radio emission at the fundamental of the plasma frequency the density at the turning point of the loop has been determined from the U burst top frequency. Considering the geometrical and density aspects we build the density model. In varying the beam and the loop magnetic field parameters we fit the observed radio data (spectrogram, radio source site distribution, and timing) with our model. For an initial electron velocity of 10^{10} cm s^{-1}, and a plausible loop top magnetic field of B = 5 G the results shown in Figure 2 are derived. Figure 2A shows the trajectories of 20 representative numerical electrons. Most of these electrons are propagating along the loop and are reflected by the magnetic mirror on the opposite side of the loop. These trajectories correspond to the gross characterictics of the observed U(N) radio burst (Figure 1). For comparison with the observed radio spectrum (Figure 1A) see Figure 2B (the synthetic radio spectrum). To explain the 2 weak subsources observed after the rising U burst branch at the injection site of the loop (Figure 1B) we consider the whistler turbulence zone with an energy level $W_w^{tot} = 5 \times 10^{-6}$ erg cm^{-3}. In the present example, the whistler turbulence region must be near the loop top, but closer to the injection site as follows from the time sequence of the observed subsources (Figure 1B). As evidenced by Figure 2A, the zone of whistler turbulence backscatters some electrons. The backmoving electrons should form a faint reverse drift burst (the first weak subsource; "1" in Figures 1B and 2A), some of these electrons are mirrored in the injection leg of the loop and just form also a secondary faint N burst branch (the second weak subsource, "2" in Figures 1B and 2A). In the spectrum these faint additional N branches are covered by the stronger main U(N) burst spectral signature.

Conclusions

1. We successfully applied our model to the U(N) burst observed at February 23, 1993.
2. Scattering of beam electrons at a zone of enhanced whistler wave turbulence near the loop top is important for understanding the observations. Considering this scattering we can explain the remarkable spatial splitting of some type U burst radio sources.

Acknowledgements

We would like to acknowledge the support of Deutsche Forschungsgemeinschaft through Grant No. DFG - Au 106/6-1 and Academy of Sciences of the Czech Republic through Grant No. 303404.

[1] Suzuki, S., Dulk G.A.: Solar Radiophysics, Cambridge University Press (1985) 289
[2] Caroubalos C., Poquérusse M., Bougeret J. L., and Crépel R.: ApJ **319** (1987) 503
[3] Karlický M., Mann, G, Aurass, H.: A&A (1996) in press
[4] Karlický M.: Sol. Phys. **145** (1993) 137
[5] Karlický M., Hénoux J.C.: A&A **278** (1993) 627
[6] Miller J.A., Ramaty R.: ApJ **344** (1989) 973
[7] Aurass H., Klein K.-L.: A&A Suppl. (1996), in press

RELATIVISTIC ELECTRON BEAM DYNAMICS IN THE PULSAR MAGNETOSPHERE

O.V. Chedia, T.A. Kahniashvili, G.Z. Machabeli and
I. S. Nanobashvili

Department of Theoretical Astrophysics, Abastumani Astrophysical Observatory, A.Kazbegi ave.2[a], 380060 Tbilisi, Republic of Georgia

Abstract

The investigation of a relativistic electron beam dynamics in the pulsar magnetosphere is given. The equation of motion of the magnetospheric plasma particles is discussed. As it turned out, if the particle radial velocity $V_r > c/\sqrt{2}$ (where c is the speed of light), centrifugal acceleration changes its sign and the particle braking begins. Also the stability of the magnetospheric plasma with respect to the radially oriented potential perturbations is discussed and the possibility of the electrostatic field generation in the pulsar magnetosphere plasma along the magnetic field lines is shown.

Introduction

As it is well known, pulsar is a rotating neutron star with the extremely high magnetic field, about $10^{12} - 10^{13}$ G. We use the perpendicular rotator model of the pulsar magnetosphere. The magnetic field lines are frozen in the pulsar so they rotate together with it as a whole. Because of the rotation of the star together with its magnetic field the electric field is generated which has the nonzero component along the magnetic field lines. This electric field ejects the particles (most of scientists think that these particles are electrons) from the pulsar surface and accelerates them up to the relativistic velocities. The particles, moving along the curved magnetic field lines, radiate γ-quanta and when their energy ε_γ exceeds electron's doubled rest energy $2mc^2$ ($\varepsilon_\gamma > 2mc^2$), γ-quantum decays into an electron-positron pair. This pair is also accelerated in the electric field and γ-quanta appear again which also decay into the electron-positron pairs, etc. Because of this cascad process the relativistic electron-positron plasma is formed in the pulsar magnetosphere. This plasma in its turn screens the electric field generated by the pulsar rotation.

We assume that the magnetic field lines are located in the plane which is perpendicular to the pulsar rotation axis. We also assume that they are radial straight lines. This assumption is justified because we discuss the processes in the magnetospheric layer the thickness of which is much less than the curvature radius of the magnetic field lines.

As we have mentioned above, the particles move along the magnetic field lines which are frozen in the pulsar and rotate together with it, thus the "solid-body type" rotation (corotation) takes place in the pulsar magnetosphere. This is the reason of the strange dynamics of the plasma particles in the pulsar magnetosphere. In particular, as it turned out, if the plasma particle radial velocity $V_r > c/\sqrt{2}$, the centifugal force changes its sign and the particle braking begins. We show that because of the plasma particle braking the electrostatic field generation along the magnetic field is possible in the pulsar magnetosphere.

Main Consideration

The equation of the motion of the magnetospheric plasma particles was discussed in the paper [1]. We use the perpendicular rotator model of the pulsar magnetosphere and treat only the polar cap. The magnetic field lines are considered as radial straight lines located in the plane which is perpendicular to the pulsar rotation axis. This assumption is justified because we discuss the processes in the magnetospheric layer the thickness of which is much less than the curvature radius of the magnetic field lines. The magnetospheric plasma particles move along the pulsar magnetic field lines and also rotate together with them because the field lines are frozen in plasma. The electric field, generated by the pulsar rotation together with its magnetic field, is screened by the magnetospheric plasma.

It is convenient to begin the discussion of the plasma particle motion in the noninertial frame of a rotating magnetic field line,which is described by the metric

$$dS^2=-(1-\Omega^2r^2)dt^2+dr^2, \tag{1}$$

where Ω is the pulsar rotation frequency. Here and below we use so called geometric units $c=G=1$.

According to the Einstein principle of equivalence, we can not tell gravitation from noninertiality. Thus for the description of particle motion in the pulsar magnetosphere the 3+1 formalism can be used. This formalism is described in [2]. According to the 3+1 formalism, the equation of motion for the particle with the mass m and charge e has the following form [2]:

$$\frac{1}{\alpha}\frac{\partial\vec{p}}{\partial t}+(\vec{V}\vec{\nabla})\vec{p}=-\gamma\frac{\vec{\nabla}\alpha}{\alpha}+\frac{e}{m}(\vec{E}+[\vec{V}\vec{B}]), \tag{2}$$

where α is the so called "lapse function" and in our case $\alpha=\sqrt{1-\Omega^2r^2}$. Here and below we use the dimensionless momentum $\vec{p}$ ($\vec{p}$ is changed by $\vec{p}/m$). We can rewrite the equation (2) for the quantities defined in the rest inertial frame:

$$\frac{\partial\vec{p}}{\partial t}+(\vec{V}\vec{\nabla})\vec{p}=-\gamma\alpha\vec{\nabla}\alpha+\frac{e}{m}(\vec{E}+[\vec{V}\vec{B}]). \tag{3}$$

Now let us discuss the motion of the plasma particles in the zeroth approximation of the weak turbulence. In the limits of this approximation the quantities which are located in the equation of motion can be presented as:

$$\vec{E}=\vec{E}_0+\vec{E}_1, \qquad \vec{B}=\vec{B}_0+\vec{B}_1, \qquad \vec{p}=\vec{p}_0+\vec{p}_1, \tag{4}$$

where $\vec{E}_0$, $\vec{B}_0$ and $\vec{p}_0$ are the basic terms and $\vec{E}_1$, $\vec{B}_1$ and $\vec{p}_1$ are the perturbations in the first approximation of the expansion over the parameter of the weak turbulence. The small parameter in the approximation of the weak turbulence for the electron-positron plasma is

$$\frac{{E_1}^2}{mn\gamma}\ll 1. \tag{5}$$

From the equation of motion in the zeroth approximation for the radial acceleration one can obtain (see also [3]):

$$\frac{d^2r}{dt^2}=\frac{\Omega^2r}{1-\Omega^2r^2}\left[1-\Omega^2r^2-2\left(\frac{dr}{dt}\right)^2\right]. \tag{6}$$

The equation (6) can be solved exactly. Using Jacobian function, the solution can be presented in the form [3]:

$$r(t)=\frac{V_{0i}}{\Omega}\frac{Sn\Omega t}{dn\Omega t}, \tag{7}$$

where Sn and dn are the Jacobian elliptical sine and modulus respectively [4], V_{0i} is the particle initial velocity. From the equation (6) it follows that if the radial velocity $V_r > 1/\sqrt{2}$, the acceleration changes its sign and the particle is not accelerated but braked (see also [3]).

In the case $V_{0i} \to 1$, using the asymptotic expression for the Jacobian function one can find [3]:

$$r(t)=\frac{V_{0i}}{\Omega}sin\Omega t. \tag{8}$$

For the radial velocity we will obtain:

$$V_{0r}=V_{0i}cos\Omega t, \tag{9}$$

from which it follows that

$$V_0{}^2=(V_{0r})^2+(V_{0\varphi})^2=const \tag{10}$$

(because of the corotation $V_{0\varphi} = \Omega r$), i.e. no energy is expending on the particle braking along the field line, the radial energy transforms to the transversal one.

As it was shown above, the relativistic plasma particles are braked in the pulsar magnetosphere, if their radial velocity $V_r > 1/\sqrt{2}$. It is very interesting to discuss the stability of such a plasma with respect to the radial perturbations. In particular we discuss the potential perturbations oriented along the magnetic field lines. The initial stage of the perturbation development can be described by the equation which is easy to obtain from (3) by substituting in it the expansion (4). For the first order terms one can obtain:

$$\frac{\partial \vec{p_1}}{\partial t}+(\vec{V_0}\vec{\nabla})\vec{p_1}=(\vec{V_0}\vec{p_1})\Omega^2\vec{r}+e\vec{E_1}. \tag{11}$$

In order to eliminate the electric field $\vec{E_1}$ from the equation (11), we use the Poisson equation and the continuity equation in the first approximation of the weak turbulence. After this, making the spatial Fourier transformation one can obtain for the radial perturbations:

$$\left[\frac{\partial}{\partial t}+ik_rV_{0r}\right]^2 p_{1r}=\frac{\Omega V_{0i}{}^2}{2}\left[\frac{\partial}{\partial t}+ik_rV_{0r}\right]p_{1r}sin2\Omega t-\frac{\omega_p{}^2}{\gamma_0}p_{1r}sin^2\Omega t, \tag{12}$$

where ω_p is the plasma frequency. From the equation (12) we will obtain the dispersion relation (see in detail [5]):

$$\omega^2=\frac{\omega_p{}^2}{2\gamma_0}-\frac{k_r{}^2V_{0i}{}^2}{2}. \tag{13}$$

We know that $E_1 \sim exp(-i\omega t)$ so one can conclude that when the second term in the right hand side of (13) is larger than the first term the aperiodic instability is developing in the pulsar magnetosphere, i.e. the field E_1 is increasing exponentially along the magnetic field lines.

The condition of the aperiodic instability development can be written in the following form:

$$l_r < \frac{V_{0i}\sqrt{\gamma_0}}{\omega_p}, \tag{14}$$

where l_r is the charge separation scale in the magnetospheric plasma. For the typical parameters of the pulsar magnetosphere the charge separation scale at the light cylinder (the light cylinder is the surface on which the azimuthal velocity equals to the speed of light $V_\varphi = \Omega r = c$) is of the order $10^6 sm$.

Conclusion

At the end let us discuss the possible results of the instability. We can see that the plasma motion along the magnetic field lines and at the same time rotation together with them (i.e. corotation) causes the generation of the aperiodically increasing electrostatic field under the condition (14). On the other hand it is selfevident that the corotation can not take place on the arbitrary distances from the pulsar surface because on some distance the azimuthal velocity will reach the speed of light $V_\varphi = \Omega r = c$. So, the corotation must be removed. The instability which was discussed above can contribute to the process of the corotation removing, in particular the increasing electric field will cause the additional braking of the particles of one sort and the decreasing of the braking of the other sort. This fact will evidently cause the motion of the electrons and the positrons with respect to each other, i.e. the increasing current $\vec{j}$ will appeare. So, according to the Maxwell equation $4\pi\vec{j}=rot\vec{B}$, the magnetic field will be generated. The current will be directed along the pulsar magnetic field lines, therefore the generated magnetic field will have the azimuthal component B_φ. The particles move along the field lines so the corotation will be removed. The electric field, i.e. the current $\vec{j}$ will increase until the corotation law removal.

[1] O.V. Chedia, T.A. Kahniashvili, G.Z. Machabeli and I.S. Nanobashvili, Astrophys. Space Sci. (in press).

[2] "Black Holes: The Membrane Paradigm" eds. K.S. Thorne, R.H. Price, D.A. Macdonald (Yale University Press, New Haven and London), 1988.

[3] G.Z. Machabeli and A.D. Rogava, Phys.Rev. **50**, 98 (1994).

[4] "Handbook of Mathematical Functions", eds. M. Abramowitz and I.A. Stegun, 1964.

[5] T.A. Kahniashvili, G.Z. Machabeli and I.S. Nanobashvili, submitted to Phys. Plasmas.